https://doi.org/10.1016/j.engfracmech.2022.108668



# Atomistic Insights into the Debonding of Epoxy–Concrete Interface with Water Presence

Ming-Feng Kai[1], Wei-Ming Ji[2], and Jian-Guo Dai[3]*

1. Research Assistant Professor, Department of Civil and Environmental Engineering, The Hong Kong Polytechnic University, Humg Hom, Kowloon, Hong Kong; Email: mingfeng.kai@polyu.edu.hk
2. Research Fellow, School of Mechanical and Aerospace Engineering, Nanyang Technogical Univeristy, Singapore; Email: weiming.ji@ntu.edu.sg
3. Professor, Department of Civil and Environmental Engineering, The Hong Kong Polytechnic University, Humg Hom, Kowloon, Hong Kong; Email: cejgdai@polyu.edu.hk (Corresponding author)

**Abstract**

In this study, molecular models are developed to investigate the water-induced bond degradation of the epoxy–concrete interface. Concrete is simulated using the C-S-H binder. The results indicate that the interfacial chemical bonds, including Ca–O, Ca–N, and H-bond, are reduced due to the existence of water at the interface. Two different roles of water molecules are characterized in the interfacial structure, including the filling and enlarging roles. The water presence degrades the interfacial bond strength and accelerates the interface debonding process, attributed to the weakened interaction between the epoxy and the C-S-H and the weakened load transfer of water molecules. The fracture position is transferred from the internal epoxy to the interface between the epoxy and the C-S-H. These atomic-level findings facilitate a better understanding of the interfacial deterioration of epoxy-bonded systems, e.g., fiber-reinforced polymer (FRP)-strengthened concrete structures with water presence at the interface.

**Keywords:** Chemical bonding; C-S-H; Epoxy; Water molecules; Interfacial debonding

## 1. Introduction

After years of service, concrete infrastructures (e.g., bridges and buildings), often face deterioration problems and may need rehabilitation and structure strengthening. Use of externally bonded (EB) fiber-reinforced polymer (FRP) composites has become a popular solution for the strengthening of concrete structures (Fig. 1a) [1-3], attributed to the many advantages, such as high strength, light weight, corrosion and fatigue resistance and ease of installation of the FRP composite materials [4-6]. However, there are also some concerns on the EB FRP technology especially when exposed to severe environments, such as those highly moist or with elevated temperature [7-11]. Significant attention has been paid to the influence of water presence on the durability of FRP-to-concrete bond interface at both macroscopic and microscopic scales, as water is one of the most often encountered deterioration factors of FRP-to-concrete interface [12-18]. Since epoxy is most often used as the bonding adhesive as well as the polymer matrix of fiber composites, the bond failure at the FRP–concrete interface under a wet environment mainly depends on the bonding between epoxy and the calcium silicate hydrates (C-S-H), which is the principal binder phase in concrete [19-21].

At the microscale, C-S-H exhibits a globular texture [22] and can adsorb water on its surface from the pore solution, usually called "physically absorbed water" [23, 24], leading to a wet epoxy–C-S-H interface [25]. The epoxy polar groups also favor the water absorption at the epoxy–C-S-H interface from the surrounding environment [26]. A schematic diagram of the interfacial bond at the macroscale and microscale is shown in Fig. 1(b). Due to the limitations in scale and precision, all existing experimental studies could only provide investigations into the phenomenological weakening effect on the epoxy–concrete interface under a wet environment [7-16, 27]. The origins of the interfacial degradation and its correlation to the water present at the interface cannot be explained by such phenomenological results and remain vastly unclear. This calls for a molecular-level investigation into the fundamental mechanisms behind the interfacial degradation phenomena (Fig. 1c) [26, 28, 29].

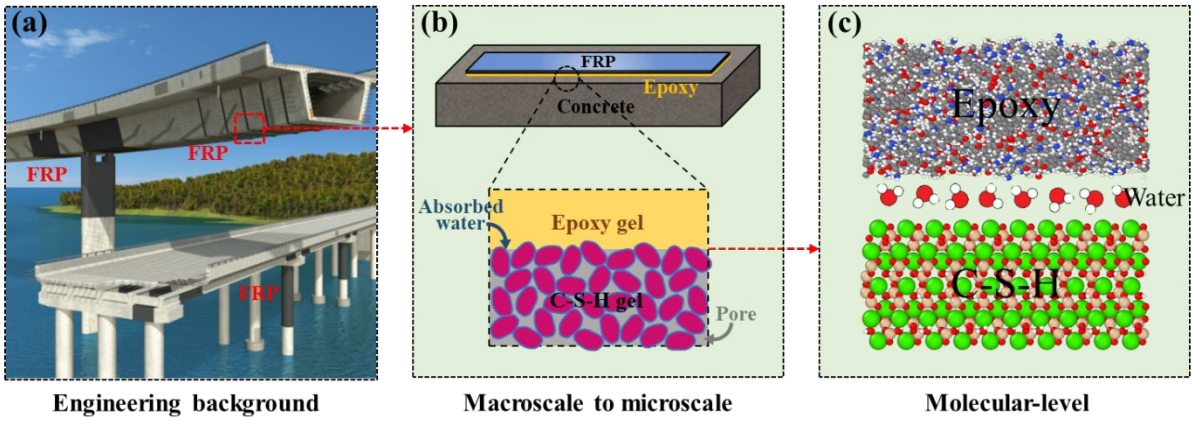


Fig. 1 (a) An example of the engineering application of FRP-strengthened concrete structure; (b) a schematic view of the macroscale FRP-to-concrete bond interface and a microscale epoxy–C-S-H interface with size down to several nanometres. The C-S-H gel exhibits globular texture at the nanoscale, and the gel particles have a strong binding ability with water from the surrounding environment. The epoxy gel also favors the water absorption on its surface due to its polar groups; (c) a schematic view of the water molecules at the epoxy–C-S-H interface at the molecular level.

Atomistic simulation, bypassing the experimental difficulties, could contribute significantly to a direct insight into materials' physical and chemical basis at the molecular level. To date, atomistic simulation has been successfully conducted to investigate the material properties of epoxy gel and C-S-H gel. Tam et al. [30] investigated the structure and binding behaviour of water molecules in cross-linked epoxy. When the water content is low, the water molecules are mainly located in the vicinity of the epoxy functional groups. By increasing the water content, the water molecules favourably form the large cluster in the epoxy. Pandiyan et al. [31] also reached similar conclusion. Honorio et al. [32] studied the pore size and temperature dependence of water diffusion in the C-S-H gel pore. The transition from glassy to Fickean-dominated dynamics occurs at an interlayer distance of 2.6 nm between two C-S-H layers. Qomi et al. [33] and Hou et al. [34, 35] reported the influence of water content on the C-S-H mechanical properties. From a dry to saturated state, the tensile strength and Young's modulus of C-S-H decrease gradually due to the water attack on the cohesive force between C-S-H layers. In addition, a few atomic-level studies have been performed to investigate the bond performance between epoxy and C-S-H gel. For example, Wang et al. [36, 37] and Hou et al.

[14] evaluated the debonding behaviour of epoxy from the C-S-H surface, and found that water and salt environment can significantly disrupt the integrity of the epoxy–C-S-H interface, and thus weaken the adhesion of epoxy on the C-S-H surface. Yu et al. [25] also reported the weakening effect of water molecules on the interfacial integrity of epoxy–C-S-H interface. These studies have facilitated a better understanding of the interfacial physics and chemistry, which are usually not accessible experimentally. However, there are still some open questions regarding how various water contents on the C-S-H affect the interfacial structures (such as the atomic interactions among these three phases) and bond properties (such as the bond degradation and fracture characteristics) between epoxy and C-S-H.

In this study, an all-atom simulation is performed to offer direct insights into the interfacial bond behaviour of the epoxy−C-S-H interface with a focus on the influence of the water presence. First, a series of interfacial molecular models are built with different water contents set at the interface. The interfacial ionic bond and hydrogen-bond (H-bond) are characterized to find how the interfacial interactions are formed. Next, the interfacial bond strength is measured by applying an external detaching force to epoxy, and the full-range fracture process of the interface is captured. The findings are expected to be useful for understanding the degradation mechanism of EB FRP systems with water presence at the interface.

## 2. Computational Methods

### 2.1 Model establishment

In the model, (10 × 8 × 1) supercell of Hamid's tobermorite-11 Å (6.69 Å × 7.39 Å × 22.77 Å, $\alpha = \beta = 90^{o}$, $\gamma = 120^{o}$), is transformed to an orthogonal molecular model (55.88 Å × 59.12 Å × 22.77 Å, $\alpha = \beta = \gamma = 90^{o}$) as the C-S-H substrate with a dry surface (Fig. 2a), following the method proposed by Tang et al. [38]. Then a layer of water is prepared by packing water molecules into a 5 Å thick box with a predefined density of 1.0 g/cm$^3$ (Fig. 5b) [39]. This layer of water is divided into five equal parts along z direction and thus different thicknesses (0, 1, 2, 3, 4 and 5 Å) of water can be chosen and placed on the C-S-H substrate to reveal the influence of different water contents at the interface on the interfacial bond properties. Next, an epoxy

molecular structure is established, which is composed of two basic units, diglycidyl ether of bisphenol A (DGEBA) resin and triethylenetetramine (TETA) as the cross-linker (Fig. 2c) [26]. The establishment method of the epoxy molecular structure follows the steps below: first, DGEBA and TETA units with a mole ratio of 2:1 are packed into a box (55.88 Å × 59.12 Å × 30 Å) with a predefined density of 1.1 g/cm$^3$; then these DGEBA and TETA molecules react with each other using a distance-based cross-linking scheme (Fig. 2c) [26, 40-43], which has been widely adopted in past decades [44-46]. The cross-linking scheme mainly involves the following steps: (1) the reactive atoms on the DGEBA resin and the cross-linker are recognized; (2) the epoxide groups (that contain the reactive atoms) on the DGEBA resin are opened, and bonded with the reactive atoms on the cross-linker via C-N bond when the reaction radius is reached; (3) the H atoms on the reacted N atoms will be removed (for charge balance), and the unreacted O atoms are saturated with H atoms (for charge balance); (4) the cross-linked epoxy is relaxed for the next reaction. The reaction radius is set to be 3 to 10 Å with an increment of 0.5 Å. After the step-by-step reaction, geometry optimization, and dynamic equilibration, a cross-linked epoxy structure can be obtained with an 80% crosslinked degree. The final density of the epoxy model is 1.13 g/cm$^3$, in the range of 1.08−1.15 g/cm$^3$ (obtained by MD analysis [47, 48]) and 1.13−1.16 g/cm$^3$ (obtained by experimental tests [49, 50]). The Young's modulus of the epoxy model is 3.75 GPa, in the range of 3.20−4.31 GPa (obtained by MD analysis [41, 51]) and close to the experimental values (3.4−3.5 GPa) [50, 52]. Finally, the epoxy structure is placed on the water zone. The initial gap width between the water zones and C-S-H substrate (or epoxy structure) is 5 Å. Fig. 2(d) presents atomic structures of epoxy–C-S-H with three different thicknesses of water at the interface.

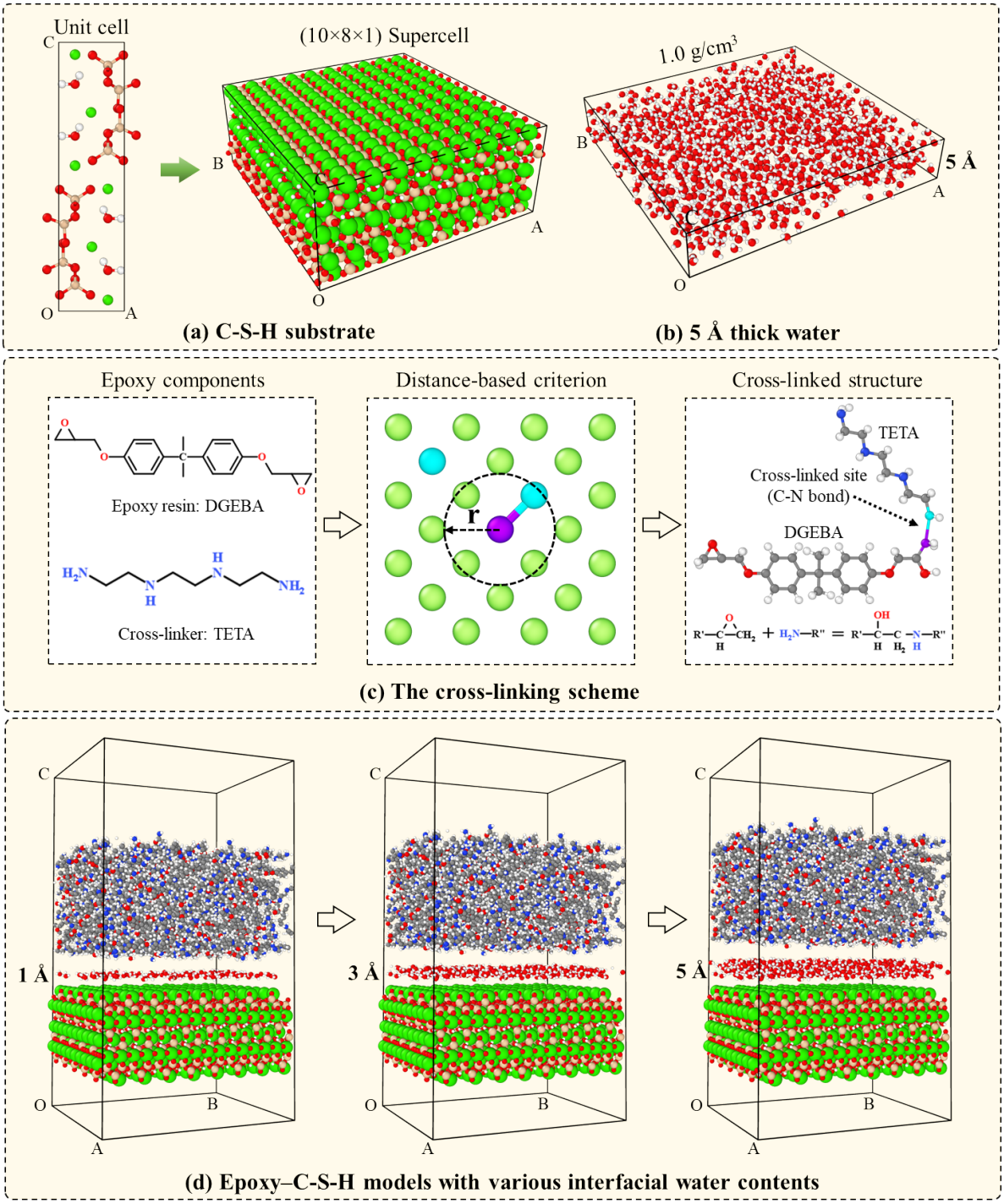


Fig.2 (a) The atomic structure of the C-S-H substrate produced from the unit cell of Hamid's tobermorite-11 Å; (b) a 5 Å thick water layer with a density of 1 g/cm$^3$; (c) a schematic view of the cross-linking scheme to realize the cross-linking between DGEBA and TETA molecules in the epoxy molecular structure; (d) the atomic structures of epoxy–C-S-H with different thicknesses of water at the interface. Vacuum gaps of 10 Å and 100 Å are created at the lower and upper of the composite models, respectively. The green, peachpuff, red, white, grey, dark blue spheres represent the Ca, Si, O, H, C and N atoms in the molecular models. In addition, the light blue

and purple spheres in Fig. 2(c) represent the C and N atoms involving in the cross-linking reaction while and the light green spheres represent all other atoms in the system.

## 2.2 Force field

The empirical force fields, including the ClayFF force field and CVFF force field, are employed to describe the interaction between atoms in epoxy–C-S-H molecular models. The Lorentz-Berthelot mixing rule [53] is applied for the combination of ClayFF and CVFF. ClayFF, a general force field suitable for simulating C-S-H systems and their interfaces with aqueous solutions, is based primarily on non-bonded interactions. The functional form of ClayFF can be represented by a sum of the electrostatic (Coulombic) interactions, the short-range interactions (the van der Waals term), and a very limited number of explicit bonded interactions to describe the bond stretching energy and angle bending energy in water molecules within C-S-H model,

$$E_{C-S-H} = E_{Coul} + E_{vdW} + E_{bond} + E_{angle} \quad (1)$$

where the parameters for Coulombic and vdW interactions were determined by density functional theory (DFT) calculations and can be obtained from Ref. [54]. CVFF, originally derived for organic molecules (amides, carboxylic acids, etc.), was proved to show a good performance in simulating epoxy molecules. The potential function in CVFF consists of the bonded interactions (bond stretching, angle bending, four-body dihedral angle torsion, and four-body improper out-of-plane terms) and non-bonded interactions (Coulombic and vdW terms),

$$E_{epoxy} = E_{bond} + E_{angle} + E_{dihedral} + E_{improper} + E_{Coul} + E_{vdW} \quad (2)$$

where the parameters for the bonded and non-bonded interactions can be obtained from Ref. [55]. The flexible SPC water model, compatible with both ClayFF and CVFF, describes the water molecules between epoxy and C-S-H. During the simulation process, the cut-off distance for vdW interactions in the epoxy–C-S-H systems is set as 10 Å, and a particle-particle particle-mesh (PPPM) solver is used to compute long-range Coulombic interactions in epoxy–C-S-H systems with an accuracy of $10^{-4}$ [26].

### 2.3 Simulation details

To start, vacuum gaps of 10 Å and 100 Å are created at the bottom and top of the composite models, respectively, to leave enough space for the pull tests [56]. The simulation process follows the steps below: first, energy minimization of the epoxy–C-S-H molecular structures is performed by iteratively optimizing the atom positions based on the conjugate gradient (CG) algorithm with the convergence criterion of $10^{-6}$ kcal/mol for energy and $10^{-6}$ kcal/(mole*Å) for force [57]. Then, a dynamic equilibration is carried out under the isothermal-isobaric (NPT) ensemble for 500 ps. The Berendsen thermostat (300 K) and barostat (1 atm in x and y directions) are employed to rescale the positions and velocities of the atoms within the simulation box as well as the box size every timestep [58]. To measure the interfacial debonding properties, a 5 Å thick upper region of epoxy binder and a 5 Å thick lower region of C-S-H are fixed, leaving the middle part dynamically equilibrated for another 500 ps. Finally, s series of tensile tests are carried out by applying a constant velocity (0.01 Å/ps) on the upper fixed region along z direction. The tensile velocity is lower enough for MD simulation to mimic the experimental quasi-static loading [26, 59]. The simulation work is conducted using the Large-scale Atomic/Molecular Massively Parallel Simulator (LAMMPS) package. A time step of 0.5 fs is chosen, and periodic boundary conditions (PBC) are applied in each dimension of the simulation box.

## 3. Results and Discussion

### 3.1 Structure evolution

The molecular structure evolution under the influence of water at the interface is essential to understand the interfacial characteristics of the epoxy–C-S-H composites [60]. First, the interfacial molecular structure of the epoxy–C-S-H with a dry interface is characterized to observe the structure evolution. Three typical interfacial bonds are existing at the interface, including Ca–O ionic bond (the C-S-H offers $Ca^{2+}$ and the epoxy offers O), Ca–N ionic bond (the C-S-H offers $Ca^{2+}$ and the epoxy offers O), and H-bond (the C-S-H offers O and the epoxy offers H), as shown in Fig. 3(a-c). The $Ca^{2+}$ ions are also ionic-bonded with the dangling O

atoms on the C-S-H surface, as shown in Fig. 3(d), which is due to the charge balance. The partial radial distribution functions, which are proportional to the probability of finding an atom at a distance from another atom [61], of Ca–O ionic bond, Ca–N ionic bond, and H-bond at the epoxy–C-S-H interface are shown in Fig. 2. The first peaks of the partial radial distribution functions correspond to the interfacial bonds, and the average bond lengths are 2.5 Å, 2.7 Å, and 1.7 Å for Ca–O bond, Ca–N bond, and H-bond, respectively. In addition, the average bond length for Ca–O (O from the C-S-H) is 2.3 Å. Based on the partial radial distribution functions, the number of interfacial bonds can be characterized.

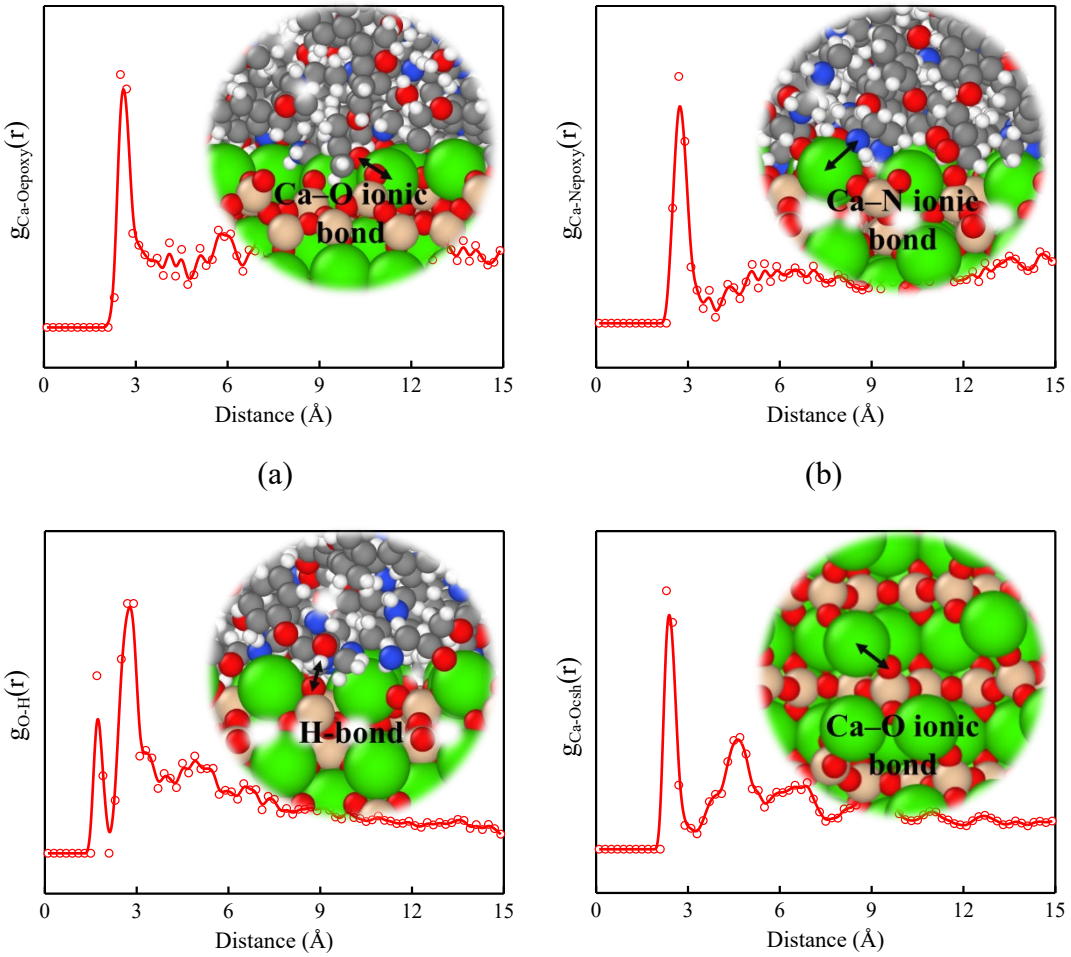


Fig. 3 (a-c) Partial radial distribution functions of Ca–O ionic bond, Ca–N ionic bond, and H-bond at the epoxy–C-S-H interface. The inset shows the snapshots of the interfacial bonds between the epoxy and the C-S-H; (d) Partial radial distribution functions of Ca–O (O from the C-S-H) ionic bond on the concrete substrate. The inset shows the snapshot of the Ca–O bond. The critical lengths for the interfacial Ca–O ionic bond, Ca–N ionic bond,

and H-bond are 3.1 Å, 3.3 Å and 2.3 Å, respectively (obtained from the RDF curves where the first peak ends), within which values the atoms can be considered to be bonded. Besides, the critical length for the Ca–O (O from the C-S-H) bond on the C-S-H surface is 3.0 Å.

Next, the concentrations of various interfacial bonds of epoxy–C-S-H composites with different water thicknesses at the interface are calculated, as shown in Fig. 4 (a-c). For the epoxy–C-S-H with a dry interface, the interfacial bond concentration follows an order of Ca–N > Ca–O > H-bond. The concentrations of both Ca–N and Ca–O bonds decrease significantly with the increasing water thickness from 0 to 3 Å and almost completely disappear with the thickness of water > 3 Å. The H-bond at the interface loses almost linearly with the increasing water thickness. It can be concluded that the increasing water at the interface leads to a gradual loss of the interfacial chemical bonds. Similarly, Wang et al. [62] observed that the chemical bond between an epoxy resin molecule and the C-S-H substrate is reduced in a wet environment. Sun et al. [63] also found that the chemical bond between two C-S-H particles is reduced by increasing the water content in the particle gap. These phenomena are in reasonable agreement with our MD analytical results. In addition, it can be also found that the water molecules also cause the variation of Ca–O (O from the C-S-H) ionic bonds on the C-S-H surface, as revealed in Fig. 4(d). The concentration of Ca–O (O from the C-S-H) ionic bonds increases with the water thickness increasing from 0 to 3 Å and then decreases with the water thickness increasing from 3 to 5 Å. To explain how the interfacial water affects the Ca–O (O from the C-S-H) ionic bonds on the C-S-H surface, the distribution of the $Ca^{2+}$ on C-S-H surface is captured in the X-Z plane, as shown in Fig. 5. When the water thickness ranges from 0 to 3 Å, the $Ca^{2+}$ ions on C-S-H surface distribute in a high z coordinate range to a low z coordinate range, i.e., the average z coordinate value decreases from 30.75 Å to 30.36 Å. Almost all the $Ca^{2+}$ ions are located below the surface line of C-S-H when the water thickness reaches 3 Å. It indicates that the $Ca^{2+}$ ions are desorbed from the epoxy surface due to the introduction of water at the interface (as revealed in Fig. 4a and b), leading to the return of $Ca^{2+}$ back to the C-S-H surface. It explains why the number of Ca–O (O from the C-S-H) ionic bonds increases with the increase of water thickness from 0 to 3 Å. When the water thickness exceeds 3 Å, some $Ca^{2+}$ ions are

desorbed from the C-S-H surface, and a higher water content leads to more $Ca^{2+}$ ions desorbed from the C-S-H surface. The average z coordinate value increases from 30.36 Å to 30.69 Å due to the desorption behavior. It explains why the concentration of Ca–O (O from the C-S-H) ionic bonds decreases with the increase of water thickness from 3 to 5 Å.

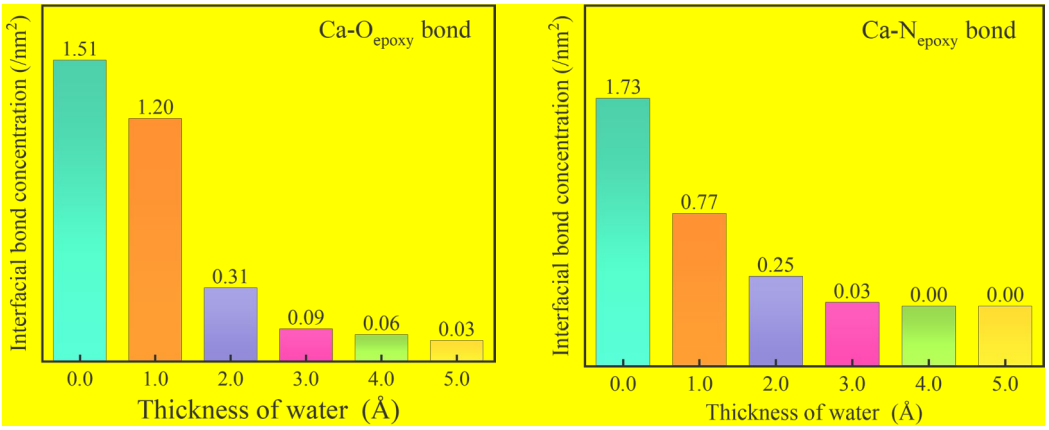


(a) (b)

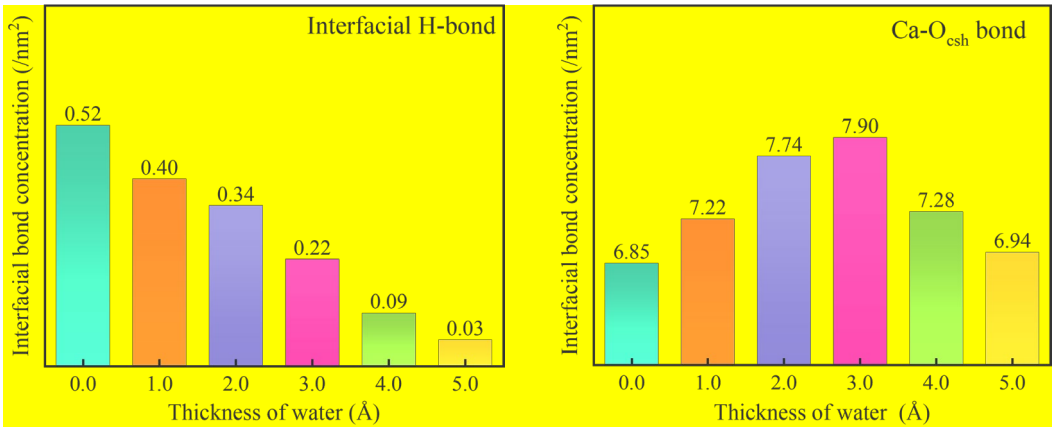


(c) (d)

Fig. 4 (a-c) The evolution of the interfacial bond concentration of Ca–O, Ca–N, and H-bond between epoxy and C-S-H substrate; (d) the evolution of the Ca–O (O from C-S-H) bond number on the C-S-H surface.

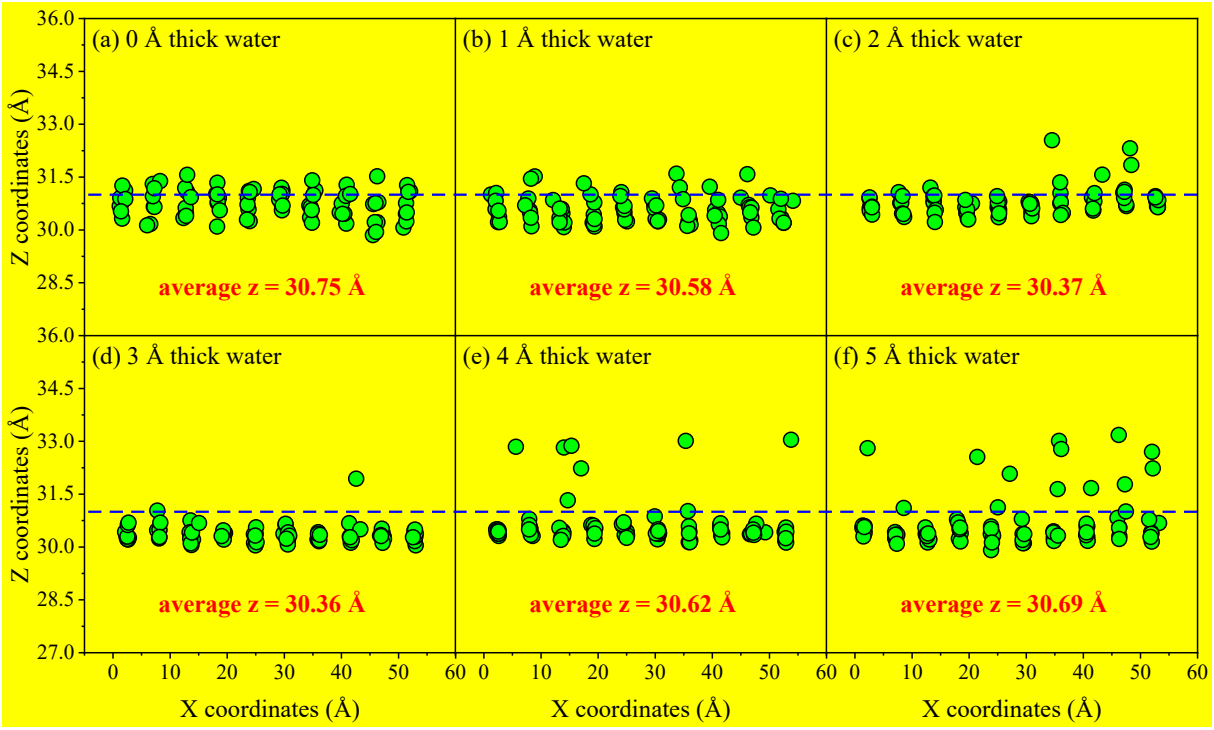


Fig. 5 The distribution of $Ca^{2+}$ on C-S-H surface in the X-Z plane for all the epoxy−C-S-H interfacial models. The average z coordinates are calculated for all the interfacial models. The blue dash lines denote the position of the C-S-H surface, where the outermost O atoms of Si-$O^-$ groups locate.

Next, the interactions between the interfacial $H_2O$ molecules and the matrices (both C-S-H and epoxy) are analyzed, as shown in Fig. 6(a). There are two bonding forms between the $H_2O$ molecules and the C-S-H matrix, including Ca–O ionic bond (the C-S-H offers $Ca^{2+}$ and the $H_2O$ offers O), and H-bond (the C-S-H offers O and the $H_2O$ offers H). For the epoxy matrix, it can only bond with the $H_2O$ molecules via H-bond. There are two types of H-bond between the $H_2O$ molecules and the epoxy matrix: one is the $H_2O$ donates the H atoms while the O or N atoms of epoxy accept the H atoms; the other is the epoxy donates the H atoms while the O atoms of $H_2O$ accept the H atoms. The bond concentration between the interfacial $H_2O$ molecules and the matrices (C-S-H and epoxy) is counted for all the atomic models, including the Ca−O bond concentration between $H_2O$ and C-S-H, the H-bond concentration between $H_2O$ and C-S-H, and the H-bond concentration between $H_2O$ and epoxy, as shown in Fig. 6(b). The concentration of Ca−O bond and H-bond between $H_2O$ and C-S-H increases gradually by introducing $H_2O$ into the epoxy–C-S-H interface. The H-bond concentration between $H_2O$ and

epoxy increases gradually when the water thickness ranges from 0 to 3 Å, and almost keeps constant when introducing more $H_2O$ into the epoxy–C-S-H interface, indicating that the H-bond between $H_2O$ and epoxy is saturated when the water thickness reaches 3 Å.

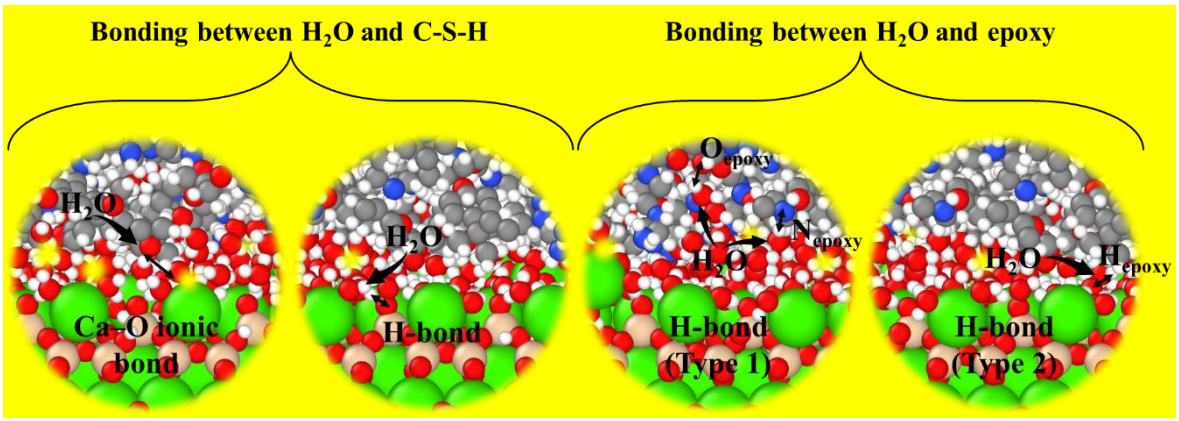


(a) Bonding between water and matrices

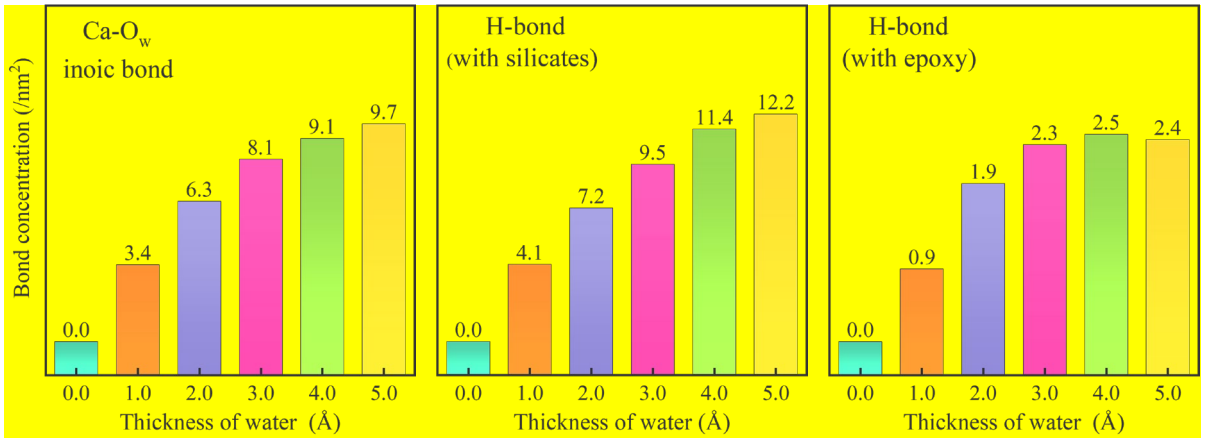


(b) The bond concentration between water and matrices

Fig. 6 (a) Snapshots of the bonding between the interfacial $H_2O$ molecules and the matrices (C-S-H and epoxy); (b) the bond concentration between the interfacial $H_2O$ molecules and the matrices (C-S-H and epoxy), including the Ca−O bond concentration between $H_2O$ and C-S-H, the H-bond concentration between $H_2O$ and C-S-H, and the H-bond concentration between $H_2O$ and epoxy.

Fig. 7(a) summarizes all the structure sizes of the epoxy–C-S-H models along the z-direction. Obviously, the water at the interface can also cause an increase in the structure size. But it is interesting to note that the magnitude of the structure size change does not agree with that of the water thickness increase at the interface. For each additional 1 Å thick water, the

evolution of the structure size is less than 1 Å, and the total change of the structure size is only 3 Å by introducing 5 Å thick water. To further understand how the water molecules change the evolution of the structure size, the atomic density profiles of the C-S-H, water, and epoxy in the epoxy–C-S-H model with 5 Å thick water is calculated as a function of the distance along the z-direction, as shown in Fig. 7(b). For comparison, the atomic density profiles of the C-S-H and epoxy in the epoxy–C-S-H model with a dry interface are also calculated. It can be seen that the distribution of water molecules overlaps with the distribution of the C-S-H atoms and the epoxy atoms. This implies that the water molecules can fill the molecular voids at the interface between the C-S-H and the epoxy, which is the reason why the structure size change is less than the thickness of water at the interface. Moreover, the distribution of the epoxy atoms in the epoxy–C-S-H model with 5 Å thick water moves to larger z-coordinates, compared with that with a dry interface. This indicates that partial water molecules involve in enlarging the interfacial space, which agrees with the results revealed in Fig. 4(a). Based on these findings, the inset in Fig. 7 shows a schematic view of two different roles of water molecules at the interface, including the filling role and the enlarging role. The filling role means that the water molecules fill in the voids at the interface, while the enlarging role means that the water molecules enlarge the interfacial space, leading to the increase in the structure size. In addition, the filling role and the enlarging role always coexist with the increasing water content at the interface, which differs from the common sense at larger scales (like macroscale) that water fills in the pores first and then enlarges the interlayer space.

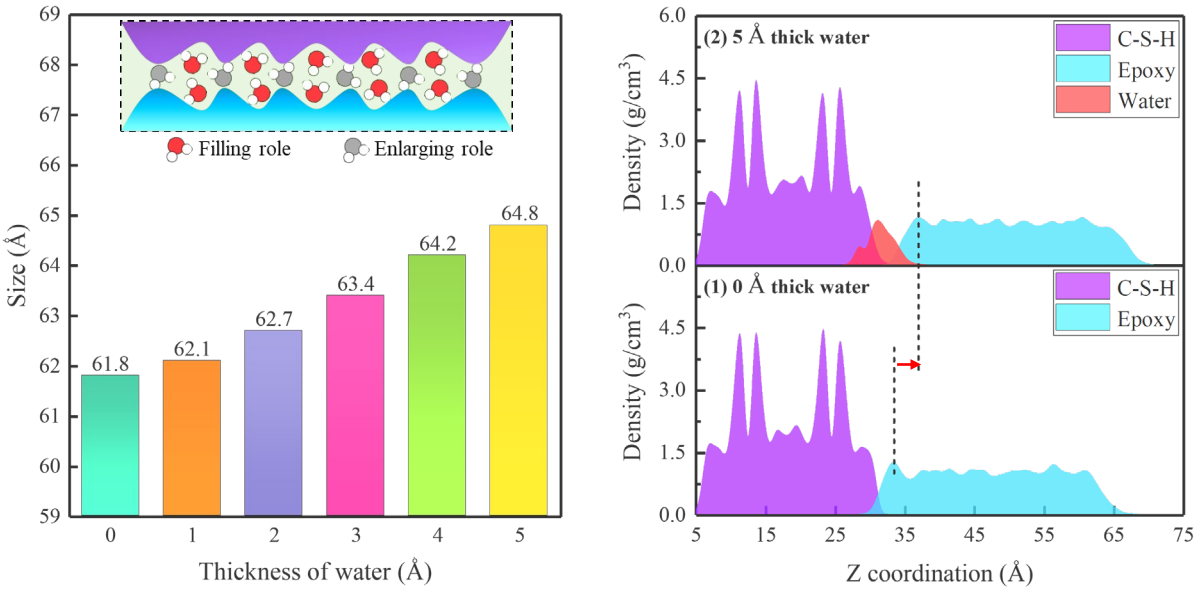


Fig. 7 (a) The structure size along z-direction for epoxy–C-S-H model with different thicknesses of water at the interface. The inset shows a schematic view of the filling role and enlarging role of water molecules at the interface; (b) the atomic density profiles of the three components of two epoxy–C-S-H models with 0 Å thick and 5 Å thick water as a function of the distance along the z-direction. The dash lines represent the position of the epoxy surface and the red arrow denotes the movement of the epoxy structure after introducing 5 Å thick water to the interface.

### 3.2 Debonding behaviors

The debonding characteristics of the epoxy–C-S-H interface with the water presence are studied by applying a constant velocity on the upper region of the epoxy structure, which is a common method to identify the debonding process between two initially bonded components [64, 65]. First, the stress-strain curves of the epoxy–C-S-H structures is recorded during the tensile tests, as shown in Fig. 8. For all the epoxy–C-S-H models, the tensile stress increases gradually at the initial stage. Then it reaches the peak, after which the tensile stress decreases gradually with further increasing of the tensile strain (the fracture stage). The peak values decrease from 287.7 to 227.5 MPa with the interfacial water thickness ranging from 0 to 5 Å, indicating that the interfacial bond strength of the epoxy–C-S-H models is weakened by water molecules, and a higher water content leads to a stronger weakening effect. It can also be found that the tensile strain at the peaks decreases from 5.7% to 4.6%, indicating that increasing the

water content at the interface causes an earlier occurrence of the fracture of the epoxy–C-S-H interface. At the fracture process, the residual bond strength also decreases with the increasing water content at the interface. For example, the tensile stress at 15% strain are 147, 89, and 45 MPa, respectively for the epoxy–C-S-H models with 0, 2, and 4 Å thick water at the interface. In summary, the interfacial water presence degrades the interfacial bond strength, the earlier occurrence of the fracture, and the lower residual bond strength. Similarly, the water presence at the asphalt–quartz interface [66], the graphene–C-S-H interface [67], and asphalt–calcite interface [64] can also lead to the interfacial mechanical degradation. Yaphary et al. [28] and Wang et al. [62] proved that the detaching force of an epoxy resin molecule from C-S-H or aggregate substrate can be decreased by water molecules. These results are in line with that in the current study.

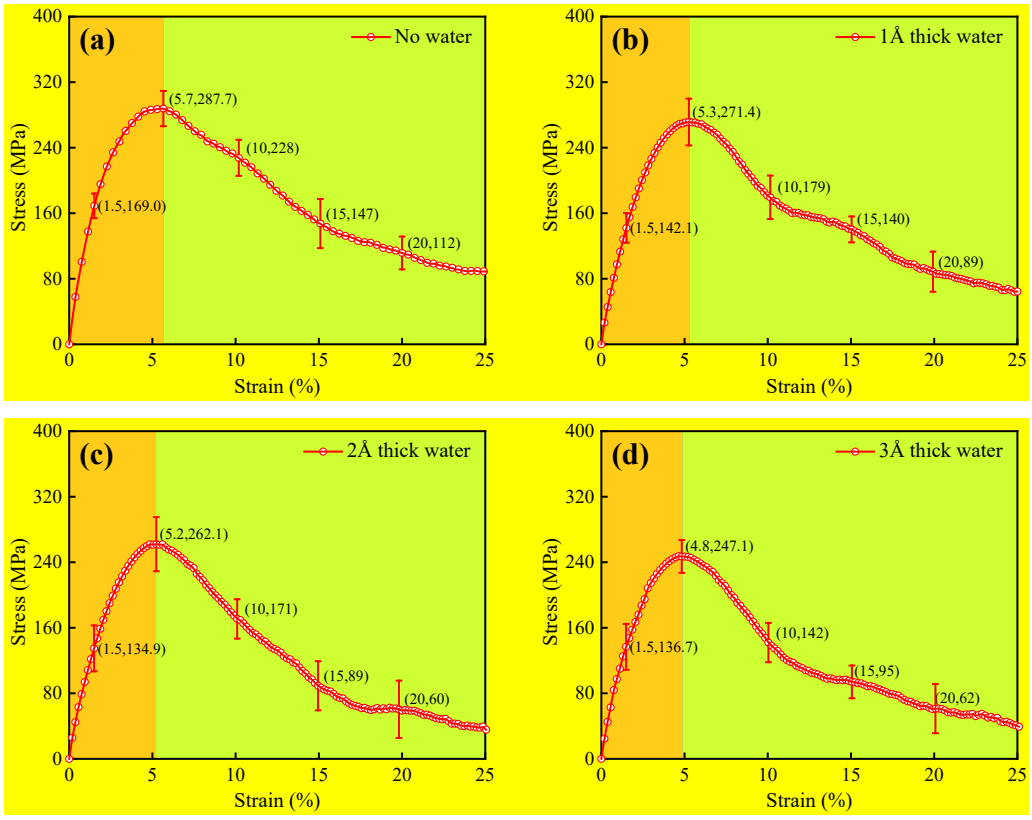

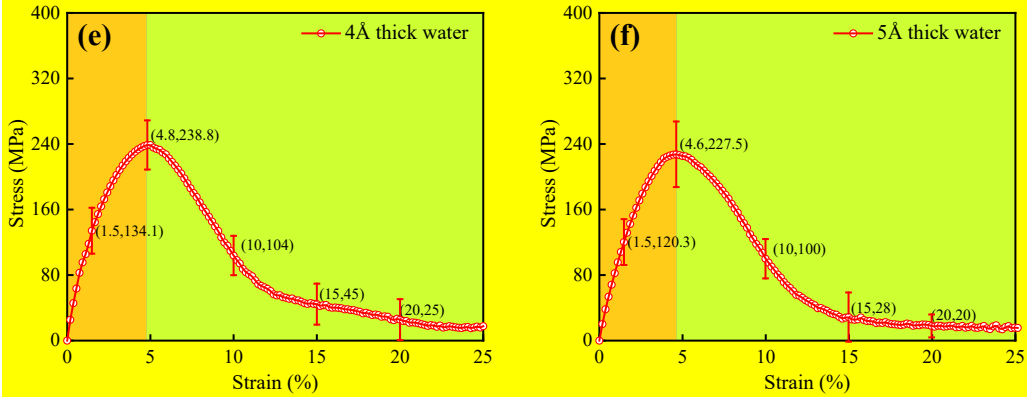


Fig. 8 The stress-strain curves of the epoxy–C-S-H models with different thicknesses of water at the interface: (a) no water; (b) 1 Å thick water; (c) 2 Å thick water; (d) 3 Å thick water; (e) 4 Å thick water; (f) 5 Å thick water. Some coordinates are labeled to reveal the relation between stress and strain at the initial stage, the peak, and the fracture stage.

Next, the snapshots of the epoxy–C-S-H models are taken during the debonding process, as shown in Fig. 9. At 5 Å displacement, some visible pores can be seen in the epoxy–C-S-H models. To investigate the influence of water on the pore formation process, the pore structures (at 5 Å displacement) are constructed via the alpha-shape method with the probe sphere radius of 5 Å [68], as shown in Fig. 10. For the dry case, no pore is formed within the interfacial model, but with gradual introduction of water into the interface the pore volume becomes larger and larger. The results reveal that the water molecules may accelerate the crack formation at the interface. By observing the whole debonding process of the epoxy–C-S-H model with a dry interface (Fig. 9a), the cracks propagate gradually with the increase of the pull displacement, and then multiple epoxy chains are observed to bridge the cracks. Afterwards, the epoxy chain bridging fails gradually, and then a singly long epoxy chain keeps bridging the cracks until the complete failure (note that there is no breakage of any covalent bond during the whole fracture process). The fracture process is similar to that of geopolymer binder–aggregate, which also undergoes crack propagation, molecular chain bridging, and failure of the chain bridging [59]. Compared with the epoxy–C-S-H model with a dry interface, it is obvious that the water presence at the interface affects the bridging of the epoxy chains, as the complete failure of the bridging occurs at the different displacements, 70 Å for the epoxy–C-S-H (a dry interface), 55

Å for the epoxy–C-S-H (1 Å thick water), 45 Å for the epoxy–C-S-H (2 Å thick water), 35 Å for the epoxy–C-S-H (3 Å thick water), 25 Å for the epoxy–C-S-H (4 Å thick water). For the epoxy–C-S-H (5 Å thick water), no epoxy chain bridging can be observed because there is almost no chemical bonding between the epoxy and the C-S-H, as reported in Fig. 4. For the epoxy–C-S-H models with 4 and 5 Å thick water at the interface (Fig. 9e and f), the water molecule chains are observed to bridge the cracks, and a higher water content leads to a longer water chain. In addition, some epoxy molecules can be pulled out by the C-S-H substrate from the epoxy structure, and the increasing water contents result in less epoxy molecules on the C-S-H substrate (Fig. 9a-d). In particular, many epoxy molecules are pulled out from the epoxy–C-S-H with a dry interface (Fig. 9a). Thus the position of the fracture can be viewed as in the internal of the epoxy structure. No epoxy molecules are found on the C-S-H substrate when the thickness of water at the interface is larger than 4 Å (Fig. 9e and f). In conclusion, the water molecules at the interface accelerate the crack formation and propagation, the failure of the epoxy chain bridging, and weaken the pull-out of the epoxy molecules by the C-S-H substrate. Moreover, the fracture plane is transferred from the internal of the epoxy to the interface with the increasing water content.

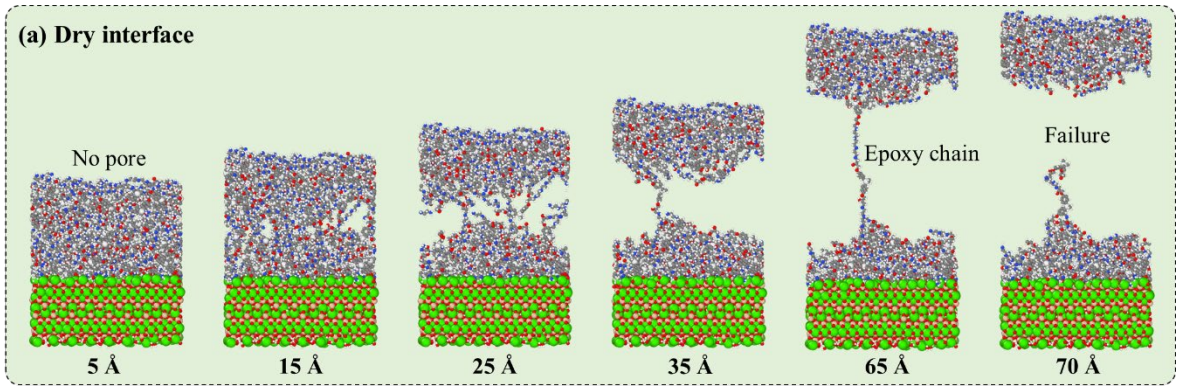

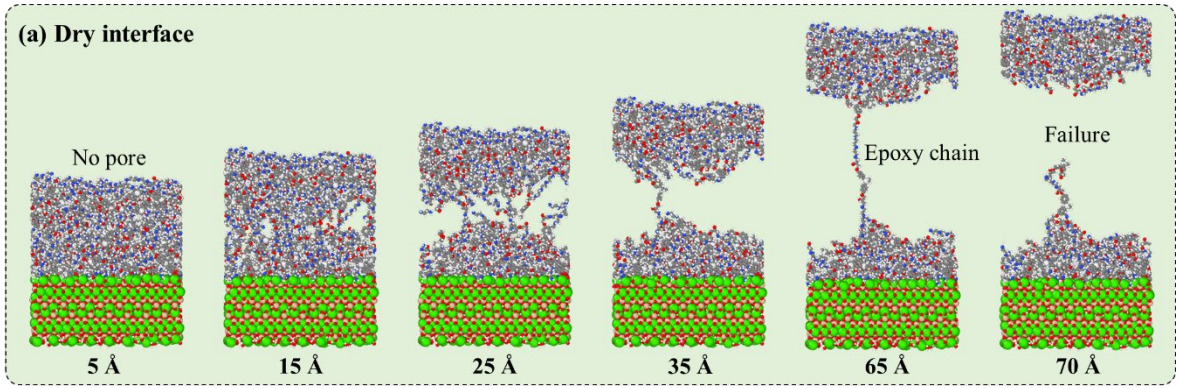


376

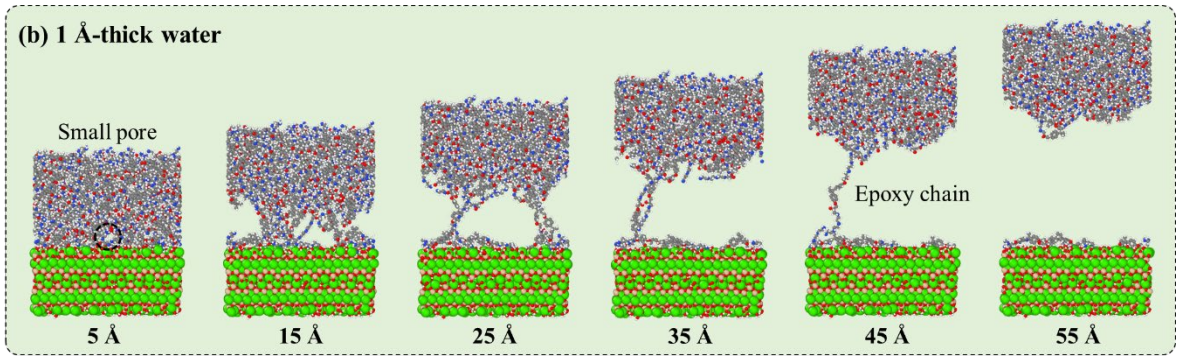


377

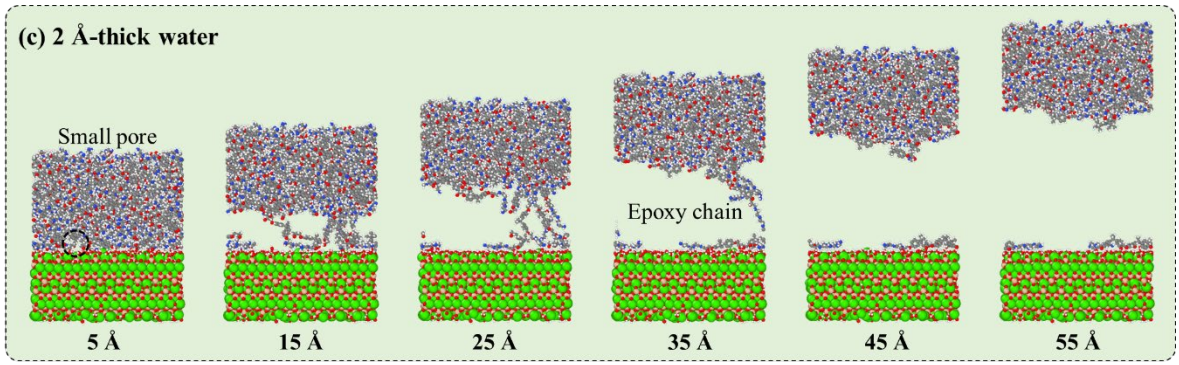


378

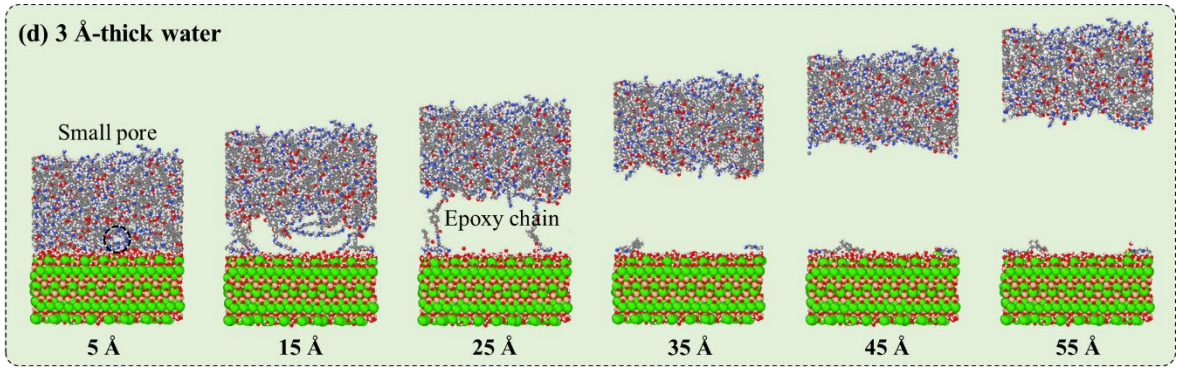


379

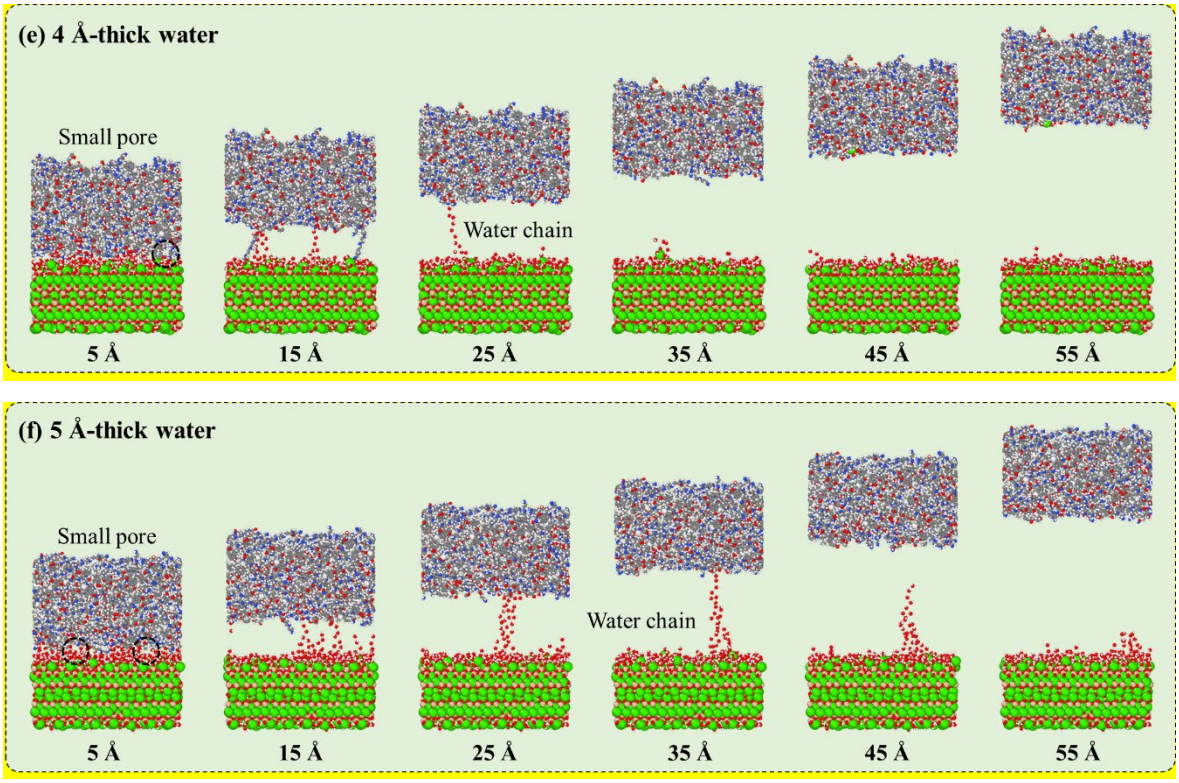


380

381

382 Fig. 9 The snapshots of the debonding process of the epoxy–C-S-H models with different water thicknesses at the

383 interface: (a) a dry interface (0 Å thick water); (b) 1 Å thick water; (c) 2 Å thick water; (d) 3 Å thick water; (e) 4

384 Å thick water; (f) 5 Å thick water.

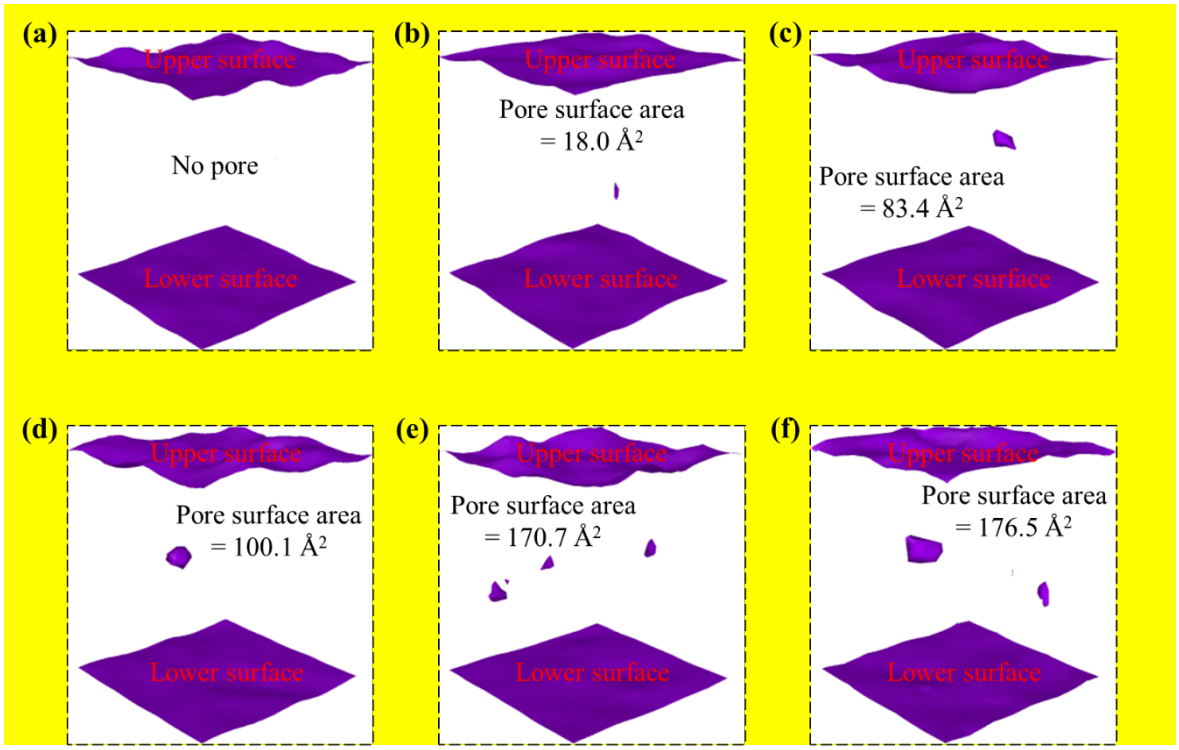


385

Fig. 10 The pore structures of the epoxy−C-S-H interfacial models with different interfacial water thicknesses at 5 Å displacement: (a) a dry interface (0 Å thick water); (b) 1 Å thick water; (c) 2 Å thick water; (d) 3 Å thick water; (e) 4 Å thick water; (f) 5 Å thick water.

To further understand how the water molecules degrade the interfacial mechanical properties, two key factors that are responsible for the mechanical strength, including the direct stress transfer between epoxy and C-S-H and the indirect stress transfer via water molecules (Fig. 11a), are analyzed. The direct stress transfer capacity is related to the interaction between epoxy and C-S-H, which can be investigated by calculating the interaction energy between these two components [59], as summarized in Fig. 11(b). The interaction energy increases significantly from -1430.7 kcal/mol to -639.9 kcal/mol when the thickness of water increases from 0 to 2 Å, then it increases to -356.3 kcal/mol with the thickness of water further increasing to 5 Å. As a lower interaction energy (more negative) corresponds to a stronger interaction, the results indicate that the increasing water content at the epoxy−C-S-H interface can weaken the interfacial interaction, leading to the decrease of the direct stress transfer capacity. Similarly, Tam et al. [69] also reported that the water presence at the epoxy−fiber interface could increase the interfacial interaction energy (less negative). In addition, the water molecules can contribute to the load transfer between the epoxy and the C-S-H. Next, to reveal the indirect stress transfer via water molecules between epoxy and C-S-H, the atom stress ($\sigma_z$) of the water molecules is calculated using the following equation [70],

$$\sigma_z = -[m{v_z}^2 + \frac{1}{2}\sum_{n=1}^{N_p}(r_{1_z}F_{1_z} + r_{2_z}F_{2_z}) + \frac{1}{2}\sum_{n=1}^{N_b}(r_{1_z}F_{1_z} + r_{2_z}F_{2_z}) + \frac{1}{3}\sum_{n=1}^{N_a}(r_{1_z}F_{1_z} + r_{2_z}F_{2_z} + r_{3_z}F_{3_z}) + Kspace(r_{i_z}, F_{i_z})]/V \quad (3)$$

where the first term is a kinetic energy contribution to atom stress; the second term is a pairwise energy contribution where $n$ loops over the $N_p$ neighbors of atoms, $r_1$ and $r_2$ are the positions of the 2 atoms in the pairwise interaction, and $F_1$ and $F_2$ are the forces on the 2 atoms due to the pairwise interaction; the third term is a bond contribution of similar form for the $N_b$ bonds which atom is part of. There are similar terms for the $N_a$ angle, which atom is part of; the last

term is the Kspace contribution from long-range Coulombic interactions; V is the atomic volume that can be approximately obtained by Voronoi analysis. The maximum atom stress of the water molecules are summarized in Fig. 11(b). The atom stress of the water molecules decreases gradually from 338.2 MPa to 239.6 MPa with the increasing water contents at the interface, indicating that higher water contents weaken the load transfer of the water molecules. Similarly, Kai et al. [71] found that the load transfer of these water molecules between two C-S-H layers is weakened by higher water contents, which is viewed as the "hydrolytic weakening mechanism". In conclusion, the degradation mechanism of the interface is attributed to two factors: one is that the direct stress transfer between epoxy and C-S-H is weakened and the other is that the indirect stress transfer via water molecules is also weakened with the presence of water at the epoxy−C-S-H interface.

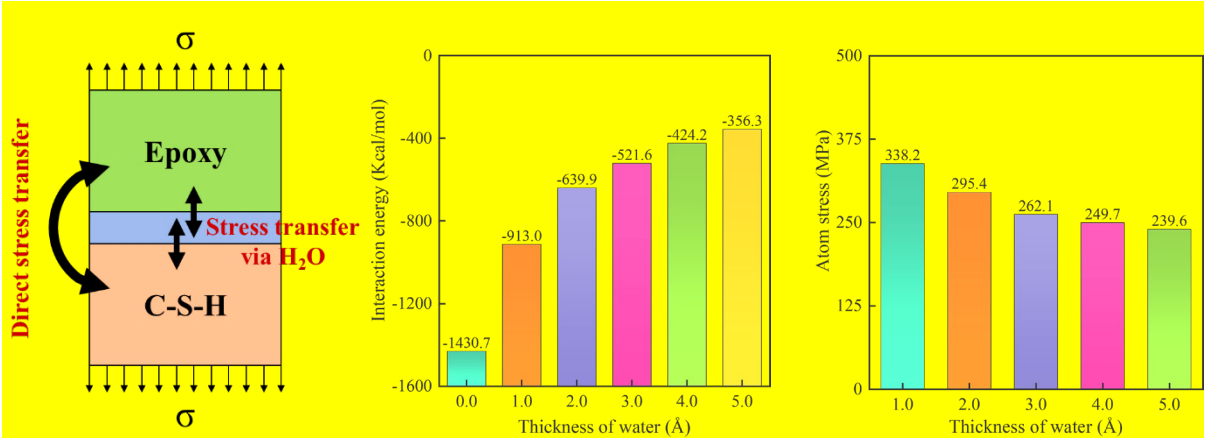


(a) (b) (c)

Fig. 11 (a) A schemetic view of the stress tranfer within the epoxy−C-S-H interfacial structures, including the direct stress transfer between epoxy and C-S-H and the indirect stress transfer via $H_2O$ molecules; (b) Summary of the interaction energy between the epoxy and the C-S-H with different thicknesses of water at the interface; (c) the maximum atom stress of the water molecules between the epoxy and the C-S-H with different thicknesses of water at the interface during the tensile tests.

Fig. 12 shows the exposed epoxy surface and C-S-H surface after the complete debonding of the epoxy–C-S-H structures (1, 3, and 5 Å thick water). It can be seen that the water molecules prefer to be absorbed by the C-S-H substrate rather than the epoxy during the debonding process. To explain this phenomenon, the interaction energy between water and

epoxy, and between water and C-S-H is calculated and shown in Fig. 12. Obviously, the C-S-H substrate has an ultra-strong water absorption ability compared to the epoxy. In addition, with the increase of the water thickness at the interface, the interaction energy per water molecule decreases, indicating that the water absorption on the C-S-H surface is weakened (physical effect: more water molecules exist at a longer distance away from the C-S-H surface). As a result, the water molecules have the possibility to be absorbed by the epoxy surface, as shown in Fig. 12(c).

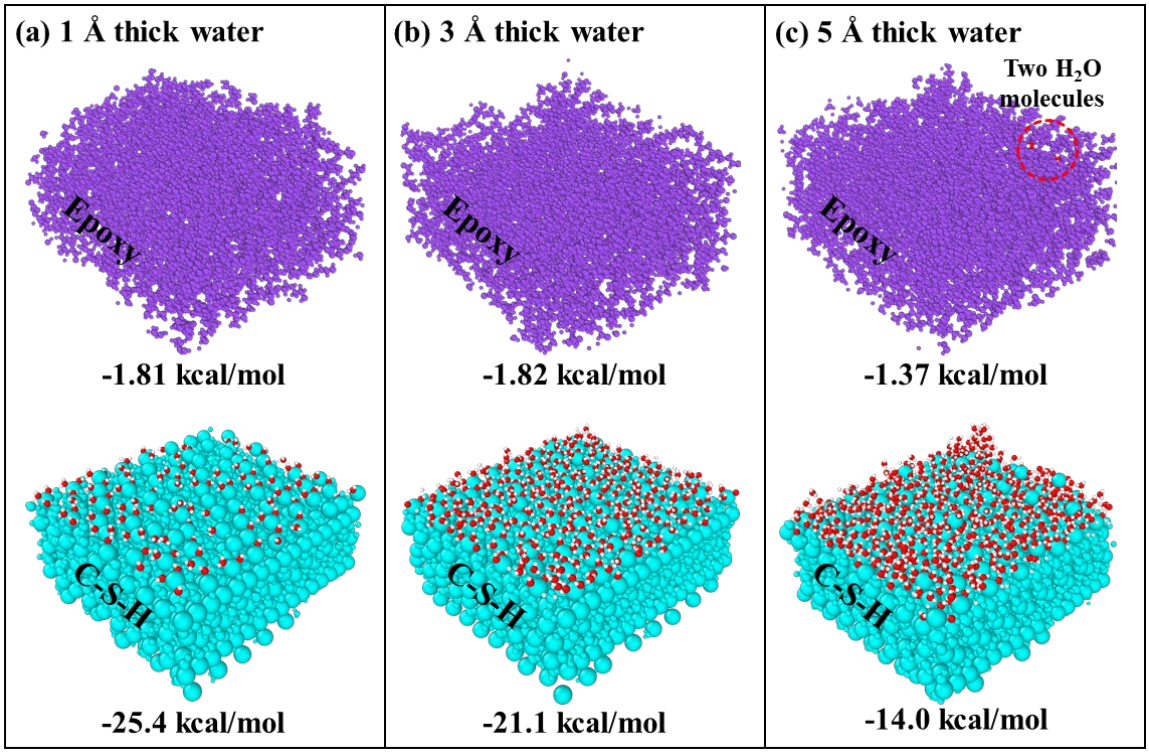


Fig. 12 The exposed epoxy surface and C-S-H surface after the complete debonding of the epoxy–C-S-H structures with 1, 3, and 5 Å thick water. The purple color is used to represent all the epoxy atoms, while the blue color is used to describe all the C-S-H atoms. The O and H in water molecules are represented in red and white colors, respectively. The data in the figure are the average values of the interaction energy between the water molecules and the epoxy and the C-S-H.

## 4. Conclusions

This study has investigated the evolution of the interfacial molecular structure and the debonding behaviour of the epoxy-to-C-S-H interface under the water presence using atomistic simulation. Some conclusions can be drawn from this research as follows:

(a) There are various forms of interfacial chemical bonding between the epoxy and the C-S-H, including Ca–O ionic bond, Ca–N ionic bond, and H-bond. All these chemical bonds decrease with the increasing water content.

(b) The size of the epoxy–C-S-H molecular structure evolves with the increasing water contents at the interface. There are two different roles of the water molecules, including the filling role and enlarging role. As only partial water molecules involve in enlarging the structure size, the increase of the structure size is smaller than the thickness of water introduced to the interface.

(c) Water can lead to the degradation of the interfacial bond strength and accelerate the crack formation and propagation, the failure of the epoxy chain bridging, and weaken the pull-out of the epoxy molecules by the C-S-H substrate. The position of the fracture is transferred from the internal of the epoxy to the interface by introducing water.

(d) The degradation mechanism of the epoxy-C-S-H interface is attributed to two factors: one is the interaction between the epoxy and the C-S-H is weakened by the water molecules, and the other is the load transfer of the water molecules becomes weaker with the increasing water content.

(e) The water molecules usually prefer to be absorbed by the C-S-H substrate rather than the epoxy during the debonding process because the former has a much stronger water absorption ability than the latter. With the increasing water content, however, a few water molecules may be absorbed by the epoxy surface.

The present work provides an atomic-level insight into the debonding performance between epoxy and C-S-H, which can be viewed as an extremely localized phnomenon in a realistic FRP-to-concrete interface. The results can also help to understand the influence of salt solutions at the epoxy−C-S-H interfaces as its main component is water, but the influence of ions in salt solutions needs to be further evaluated. However, the realistic FRP-to-concrete interface is more complicated, as concrete is a porous multiphase material that involves in a series of physical and chemical events and the moisture ingress may not only occur at the interface between epoxy and C-S-H. Although the present MD modelling can help understand

the mechanism of how the presence of water degrades the interface bond between the epoxy and C-S-H, further research is needed to correlate the atomic level behaviour to the macroscale behaviour in terms of failure mode and mechanical responses.

## Declaration of competing interest

The authors declare that they have no known competing financial interests or personal relationships that could have appeared to influence the work reported in this paper.

## Acknowledgments

The authors acknowledge the financial support received from Chinese Guangdong Province R&D Plan for Key Areas (Project No. 2019B111107002), Hong Kong Research Grants Council – Theme-based Research Scheme (Project No. T22-502/18-R), the Hong Kong-Guangzhou Technology and Innovation Partnership Program (Project No. 201807010055), and the National Natural Science Foundation of China (NSFC) Project (Project No. 51478406).

## References


[1] M. Abedini, C. Zhang, Dynamic performance of concrete columns retrofitted with FRP using segment pressure technique, Composite Structures, 260 (2021) 113473.

[2] B. Wan, C. Jiang, Y.-F. Wu, Effect of defects in externally bonded FRP reinforced concrete, Construction and Building Materials, 172 (2018) 63-76.

[3] X. Zou, P. Feng, Y. Bao, J. Wang, H. Xin, Experimental and analytical studies on shear behaviors of FRP-concrete composite sections, Engineering Structures, 215 (2020) 110649.

[4] T. Siwowski, M. Rajchel, Structural performance of a hybrid FRP composite–lightweight concrete bridge girder, Composites Part B: Engineering, 174 (2019) 107055.

[5] X. Zou, H. Lin, P. Feng, Y. Bao, J. Wang, A review on FRP-concrete hybrid sections for bridge applications, Composite Structures, DOI (2020) 113336.

[6] F.M. Mukhtar, R.M. Faysal, A review of test methods for studying the FRP-concrete interfacial bond behavior, Construction and Building Materials, 169 (2018) 877-887.

[7] J.-G. Dai, H. Yokota, M. Iwanami, E. Kato, Experimental investigation of the influence of moisture on the bond behavior of FRP to concrete interfaces, Journal of Composites for Construction, 14 (2010) 834-844.

[8] W.-Y. Gao, J.-G. Dai, J. Teng, Analysis of Mode II debonding behavior of fiber-reinforced polymer-to-substrate bonded joints subjected to combined thermal and mechanical loading, Engineering Fracture Mechanics, 136 (2015) 241-264.

[9] Z. Wang, J.-G. Dai, M. Wang, L. Chen, F. Zhang, Q. Xu, Residual bond strengths of epoxy and cement-bonded CFRP reinforcements to concrete interfaces after elevated temperature exposure, Fire Safety Journal, DOI (2021) 103393.

[10] D.-G. Jia, W.-Y. Gao, D.-X. Duan, J. Yang, J.-G. Dai, Full-range behavior of FRP-to-concrete bonded joints subjected to combined effects of loading and temperature variation, Engineering Fracture Mechanics, 254 (2021) 107928.

[11] F. Zhang, J.-G. Dai, Z. Wang, M. Wang, Y. Leng, Q. Xu, Bond durability of epoxy and cement-bonded CFRP reinforcement to concrete interfaces subject to water immersion, Materials and Structures, 54 (2021) 1-12.

[12] J. Shrestha, D. Zhang, T. Ueda, Durability performances of carbon fiber–reinforced polymer and concrete-bonded systems under moisture conditions, Journal of composites for construction, 20 (2016) 04016023.

[13] Z. Ouyang, B. Wan, Nonlinear deterioration model for bond interfacial fracture energy of FRP-concrete joints in moist environments, Journal of Composites for Construction, 13 (2009) 53-63.

[14] D. Hou, Q. Yang, P. Wang, Z. Jin, M. Wang, Y. Zhang, X. Wang, Unraveling disadhesion mechanism of epoxy/CSH interface under aggressive conditions, Cement and Concrete Research, 146 (2021) 106489.

[15] B. Ferracuti, M. Savoia, C. Mazzotti, Interface law for FRP–concrete delamination, Composite structures, 80 (2007) 523-531.

[16] H. Diab, Z. Wu, Nonlinear constitutive model for time-dependent behavior of FRP-concrete interface, Composites science and technology, 67 (2007) 2323-2333.

[17] A. Zhou, O. Büyüköztürk, D. Lau, Debonding of concrete-epoxy interface under the coupled effect of moisture and sustained load, Cement and Concrete Composites, 80 (2017) 287-297.
[18] B. Wan, M.F. Petrou, K.A. Harries, The effect of the presence of water on the durability of bond between CFRP and concrete, Journal of Reinforced Plastics and Composites, 25 (2006) 875-890.
[19] C. Tuakta, O. Büyüköztürk, Deterioration of FRP/concrete bond system under variable moisture conditions quantified by fracture mechanics, Composites Part B: Engineering, 42 (2011) 145-154.
[20] I. Alachek, N. Reboul, B. Jurkiewiez, Bond strength's degradation of GFRP-concrete elements under aggressive exposure conditions, Construction and Building Materials, 179 (2018) 512-525.
[21] S. Amidi, J. Wang, Subcritical debonding of FRP-to-concrete bonded interface under synergistic effect of load, moisture, and temperature, Mechanics of Materials, 92 (2016) 80-93.
[22] M.F. Kai, L.W. Zhang, K.M. Liew, New insights into creep characteristics of calcium silicate hydrates at molecular level, Cement and Concrete Research, 142 (2021) 106366.
[23] M. Kai, L. Zhang, K. Liew, New insights into creep characteristics of calcium silicate hydrates at molecular level, Cement and Concrete Research, 142 (2021) 106366.
[24] P. Bonnaud, Q. Ji, B. Coasne, R.-M. Pellenq, K. Van Vliet, Thermodynamics of water confined in porous calcium-silicate-hydrates, Langmuir, 28 (2012) 11422-11432.
[25] Z. Yu, A. Zhou, W. Ning, L.-h. Tam, Molecular insights into the weakening effect of water on cement/epoxy interface, Applied Surface Science, 553 (2021) 149493.
[26] X.Q. Wang, W. Jian, O. Buyukozturk, C.K. Leung, D. Lau, Degradation of epoxy/glass interface in hygrothermal environment: An atomistic investigation, Composites Part B: Engineering, 206 (2021) 108534.
[27] A. Morshedifard, S. Masoumi, M.A. Qomi, Nanoscale origins of creep in calcium silicate hydrates, Nature communications, 9 (2018) 1-10.
[28] Y.L. Yaphary, Z. Yu, R.H. Lam, D. Hui, D. Lau, Molecular dynamics simulations on adhesion of epoxy-silica interface in salt environment, Composites Part B: Engineering, 131 (2017) 165-172.
[29] L.-h. Tam, A. Zhou, Z. Yu, Q. Qiu, D. Lau, Understanding the effect of temperature on the interfacial behavior of CFRP-wood composite via molecular dynamics simulations, Composites Part B: Engineering, 109 (2017) 227-237.
[30] L.-h. Tam, D. Lau, C. Wu, Understanding interaction and dynamics of water molecules in the epoxy via molecular dynamics simulation, Molecular Simulation, 45 (2019) 120-128.
[31] S. Pandiyan, J. Krajniak, G. Samaey, D. Roose, E. Nies, A molecular dynamics study of water transport inside an epoxy polymer matrix, Computational Materials Science, 106 (2015) 29-37.
[32] T. Honorio, H. Carasek, O. Cascudo, Water self-diffusion in CSH: Effect of confinement and temperature studied by molecular dynamics, Cement and Concrete Research, 155 (2022) 106775.
[33] M.A. Qomi, K. Krakowiak, M. Bauchy, K. Stewart, R. Shahsavari, D. Jagannathan, D.B. Brommer, A. Baronnet, M.J. Buehler, S. Yip, Combinatorial molecular optimization of cement hydrates, Nature communications, 5 (2014) 1-10.
[34] D. Hou, H. Ma, Y. Zhu, Z. Li, Calcium silicate hydrate from dry to saturated state: Structure, dynamics and mechanical properties, Acta materialia, 67 (2014) 81-94.
[35] D. Hou, J. Yu, Z. Jin, A. Hanif, Molecular dynamics study on calcium silicate hydrate subjected to tension loading and water attack: structural evolution, dynamics degradation and reactivity mechanism, Physical Chemistry Chemical Physics, 20 (2018) 11130-11144.

[36] P. Wang, Q. Yang, Z. Jin, D. Hou, M. Wang, Effects of water and ions on bonding behavior between epoxy and hydrated calcium silicate: a molecular dynamics simulation study, Journal of Materials Science, 56 (2021) 16475-16490.
[37] P. Wang, Q. Yang, M. Wang, D. Hou, Z. Jin, P. Wang, J. Zhang, Theoretical investigation of epoxy detachment from CSH interface under aggressive environment, Construction and Building Materials, 264 (2020) 120232.
[38] S. Tang, A. Hubao, J. Chen, W. Yu, P. Yu, E. Chen, H. Deng, Z. He, The interactions between water molecules and CSH surfaces in loads-induced nanopores: A molecular dynamics study, Applied Surface Science, 496 (2019) 143744.
[39] R.J.-M. Pellenq, A. Kushima, R. Shahsavari, K.J. Van Vliet, M.J. Buehler, S. Yip, F.-J. Ulm, A realistic molecular model of cement hydrates, Proceedings of the National Academy of Sciences, 106 (2009) 16102-16107.
[40] L.-h. Tam, D. Lau, A molecular dynamics investigation on the cross-linking and physical properties of epoxy-based materials, RSC Advances, 4 (2014) 33074-33081.
[41] W. Jian, D. Lau, Understanding the effect of functionalization in CNT-epoxy nanocomposite from molecular level, Composites Science and Technology, 191 (2020) 108076.
[42] W.-M. Ji, L.-W. Zhang, K. Liew, Understanding interfacial interaction characteristics of carbon nitride reinforced epoxy composites from atomistic insights, Carbon, 171 (2021) 45-54.
[43] F. Jeyranpour, G. Alahyarizadeh, B. Arab, Comparative investigation of thermal and mechanical properties of cross-linked epoxy polymers with different curing agents by molecular dynamics simulation, Journal of Molecular Graphics and Modelling, 62 (2015) 157-164.
[44] D. Doherty, B. Holmes, P. Leung, R. Ross, Polymerization molecular dynamics simulations. I. Cross-linked atomistic models for poly (methacrylate) networks, Computational and Theoretical Polymer Science, 8 (1998) 169-178.
[45] C. Wu, W. Xu, Atomistic molecular modelling of crosslinked epoxy resin, Polymer, 47 (2006) 6004-6009.
[46] V. Varshney, S.S. Patnaik, A.K. Roy, B.L. Farmer, A molecular dynamics study of epoxy-based networks: cross-linking procedure and prediction of molecular and material properties, Macromolecules, 41 (2008) 6837-6842.
[47] A. Shokuhfar, B. Arab, The effect of cross linking density on the mechanical properties and structure of the epoxy polymers: molecular dynamics simulation, Journal of molecular modeling, 19 (2013) 3719-3731.
[48] F. Aghadavoudi, H. Golestanian, Y. Tadi Beni, Investigating the effects of resin crosslinking ratio on mechanical properties of epoxy - based nanocomposites using molecular dynamics, Polymer Composites, 38 (2017) E433-E442.
[49] F.G. Garcia, B.G. Soares, V.J. Pita, R. Sánchez, J. Rieumont, Mechanical properties of epoxy networks based on DGEBA and aliphatic amines, Journal of Applied Polymer Science, 106 (2007) 2047-2055.
[50] E.N. Brown, S.R. White, N.R. Sottos, Fatigue crack propagation in microcapsule-toughened epoxy, Journal of materials science, 41 (2006) 6266-6273.

[51] W. Jian, X. Wang, H. Lu, D. Lau, Molecular dynamics simulations of thermodynamics and shape memory effect in CNT-epoxy nanocomposites, Composites Science and Technology, 211 (2021) 108849.
[52] J. Wan, B. Gan, C. Li, J. Molina-Aldareguia, E.N. Kalali, X. Wang, D.-Y. Wang, A sustainable, eugenol-derived epoxy resin with high biobased content, modulus, hardness and low flammability: Synthesis, curing kinetics and structure–property relationship, Chemical Engineering Journal, 284 (2016) 1080-1093.
[53] P. Wang, G. Qiao, Y. Zhang, D. Hou, J. Zhang, M. Wang, X. Wang, X. Hu, Molecular dynamics simulation study on interfacial shear strength between calcium-silicate-hydrate and polymer fibers, Construction and Building Materials, 257 (2020) 119557.
[54] R.T. Cygan, J.-J. Liang, A.G. Kalinichev, Molecular models of hydroxide, oxyhydroxide, and clay phases and the development of a general force field, The Journal of Physical Chemistry B, 108 (2004) 1255-1266.
[55] P. Dauber-Osguthorpe, V. Roberts, D. Osguthorpe, J. Wolff, M. Genest, AT and Hagler. Structure and energetics of ligand binding to proteins: Escherichia coli dihydrofolate reductase-trimethorprim, a drug-receptor system, Proteins: Structure, Function, and Genetics, 4 (1988) 31-47.
[56] M. Kai, L. Zhang, K. Liew, Graphene and graphene oxide in calcium silicate hydrates: Chemical reactions, mechanical behavior and interfacial sliding, Carbon, 146 (2019) 181-193.
[57] M.F. Kai, L.W. Zhang, K.M. Liew, Graphene and graphene oxide in calcium silicate hydrates: Chemical reactions, mechanical behavior and interfacial sliding, Carbon, 146 (2019) 181-193.
[58] Z. Diao, Y. Zhao, B. Chen, C. Duan, S. Song, ReaxFF reactive force field for molecular dynamics simulations of epoxy resin thermal decomposition with model compound, Journal of Analytical and Applied Pyrolysis, 104 (2013) 618-624.
[59] M.-F. Kai, J.-G. Dai, Understanding geopolymer binder-aggregate interfacial characteristics at molecular level, Cement and Concrete Research, 149 (2021) 106582.
[60] F. Jiang, Q. Yang, Y. Wang, P. Wang, D. Hou, Z. Jin, Insights on the adhesive properties and debonding mechanism of CFRP/concrete interface under sulfate environment: From experiments to molecular dynamics, Construction and Building Materials, 269 (2021) 121247.
[61] D. Hou, J. Zhang, W. Pan, Y. Zhang, Z. Zhang, Nanoscale mechanism of ions immobilized by the geopolymer: A molecular dynamics study, Journal of Nuclear Materials, 528 (2020) 151841.
[62] P. Wang, Q. Yang, Z. Jin, D. Hou, M. Wang, Effects of water and ions on bonding behavior between epoxy and hydrated calcium silicate: a molecular dynamics simulation study, Journal of Materials Science, DOI (2021) 1-16.
[63] J. Sun, W. Zhang, J. Zhang, D. Hou, Molecular dynamics study the structure, bonding, dynamic and mechanical properties of calcium silicate hydrate with ultra-confined water: Effects of nanopore size, Construction and Building Materials, 280 (2021) 122477.
[64] W. Sun, H. Wang, Moisture effect on nanostructure and adhesion energy of asphalt on aggregate surface: A molecular dynamics study, Applied Surface Science, 510 (2020) 145435.
[65] S. Zhou, N. Vu-Bac, B. Arash, H. Zhu, X. Zhuang, Interface characterization between polyethylene/silica in engineered cementitious composites by molecular dynamics simulation, Molecules, 24 (2019) 1497.

[66] H. Wang, E. Lin, G. Xu, Molecular dynamics simulation of asphalt-aggregate interface adhesion strength with moisture effect, International Journal of Pavement Engineering, 18 (2017) 414-423.
[67] T. Yang, Y. Jia, D. Hou, H. Li, J. Jiang, J. Zhang, Molecular dynamics study on the weakening effect of moisture content on graphene oxide reinforced cement composite, Chemical Physics Letters, 708 (2018) 177-182.
[68] A. Stukowski, Computational analysis methods in atomistic modeling of crystals, Jom, 66 (2014) 399-407.
[69] L.-h. Tam, L. He, C. Wu, Molecular dynamics study on the effect of salt environment on interfacial structure, stress, and adhesion of carbon fiber/epoxy interface, Composite Interfaces, 26 (2019) 431-447.
[70] D. Surblys, H. Matsubara, G. Kikugawa, T. Ohara, Application of atomic stress to compute heat flux via molecular dynamics for systems with many-body interactions, Physical Review E, 99 (2019) 051301.
[71] M. Kai, L. Zhang, K. Liew, Atomistic insights into structure evolution and mechanical property of calcium silicate hydrates influenced by nuclear waste caesium, Journal of Hazardous Materials, 411 (2021) 125033.